Featured in Physics

Structural Evidence for the Spin Collapse in High Pressure Solid Oxygen

Federico Aiace Gorelli*
Shanghai Advanced Research in Physical Sciences (SHARPS), Shanghai, China;
Center for High Pressure Science and Technology Advanced Research, 1690 Cailun Road, Shanghai 201203, China;
Istituto Nazionale di Ottica, Consiglio Nazionale delle Ricerche (CNR-INO), via Nello Carrara 1, 50019 Sesto Fiorentino, Italy;
and European Laboratory for Non Lnear Spectroscopy (LENS), via Nello Carrara 1, 50019 Sesto Fiorentino, Italy

Philip Dalladay-Simpson†
Center for High Pressure Science and Technology Advanced Research, 1690 Cailun Road, Shanghai 201203, China

Gaston Garbarino and Mohamed Mezouar
European Synchrotron Radiation Facility, 71 Avenue des Martyrs, Grenoble 38000, France

Julien Haines‡
Institute Charles Gerhardt Montpellier (ICGM), University Montpellier, CNRS, ENSCM, 34293 Montpellier, France

Mario Santoro§
Istituto Nazionale di Ottica, Consiglio Nazionale delle Ricerche (CNR-INO), via Nello Carrara 1, 50019 Sesto Fiorentino, Italy
and European Laboratory for Non Linear Spectroscopy (LENS), via Nello Carrara 1, 50019 Sesto Fiorentino, Italy

(Received 4 December 2024; revised 20 May 2025; accepted 2 June 2025; published 12 August 2025)

Single crystal x-ray diffraction measurements have been carried out on epsilon oxygen up to 30 GPa to examine the behavior of the constituent $(O_2)_4$ units. An isostructural phase transition is evidenced by lattice parameter and intracluster (O_8) distance discontinuities and clear changes in the equation of state at 18.1 ± 0.5 GPa on compression. This transition corresponds well to the predicted collapse of the molecular magnetic moment from spin-liquid, ϵ_1, to a spinless, ϵ_0, states of the O_8 structure. The collapse of the molecular magnetic moment has to date only been supported by spectroscopic data and, until now, has not been substantiated structurally.

DOI: 10.1103/jvd7-v9h9

Oxygen is unique among simple diatomic molecules in possessing a molecular spin ($S = 1$) in its ground state, leading to a rich solid-state phase diagram at low pressures (see Fig. 1) [1,2]. Unlike N_2, H_2, and F_2, liquid oxygen is paramagnetic, that is, it appears blue due to triplet-singlet electronic transitions, and can be trapped in magnetic fields. Solid oxygen represents the only known insulating elemental antiferromagnet, with intramolecular spin-orbit coupling aligning spins perpendicular to molecular axes. Intermolecular exchange interactions organize O_2 molecules parallel to each other (except in rotationally free γ-O_2) and perpendicular to basal planes. These interactions are strongly anisotropic, being dominant within basal planes while interplanar coupling is weak enough to enable 2D modeling. Below 10 GPa, magnetic ordering varies across phases (see Fig. 1) due to competition between elastic and magnetic forces. Elastic interactions favor triangular β-O_2 packing with short-range frustrated antiferromagnetism, while magnetic forces drive long-range order in α-O_2 and δ-O_2. The latter induces basal plane distortions that increase the b/a ratio [3] (see Fig. 1).

Antiferromagnetic solid oxygen is a prototypical Mott-Hubbard insulator, governed by strong intramolecular Coulomb repulsion ($U \sim 10$ eV) within the π^* state [6]. At high pressures, however, intermolecular charge transfer and band formation are expected to drive metallization via magnetic collapse, producing a nonmagnetic metal. Early density-functional theory (DFT) calculations within the local spin density approximation supported this picture [7], yet they failed to predict two key experimental observations: the significantly higher metallization pressure and the unexpected stability of the insulating ϵ-O_2 phase (8–96 GPa) [8–12]. This ϵ phase arises from a unique molecular clustering mechanism [13], forming $(O_2)_4$ tetramers [14–16] stabilized by intermolecular bonds. Theoretical work suggests this structural reorganization resembles a 2D Peierls distortion [17], which explains both the emergent band structure and the striking red color [18]

*Contact author: federico.gorelli@sharps.ac.cn
†Contact author: philip.dalladay-simpson@hpstar.ac.cn
‡Contact author: julien.haines@umontpellier.fr
§Contact author: mario.santoro@ino.cnr.it

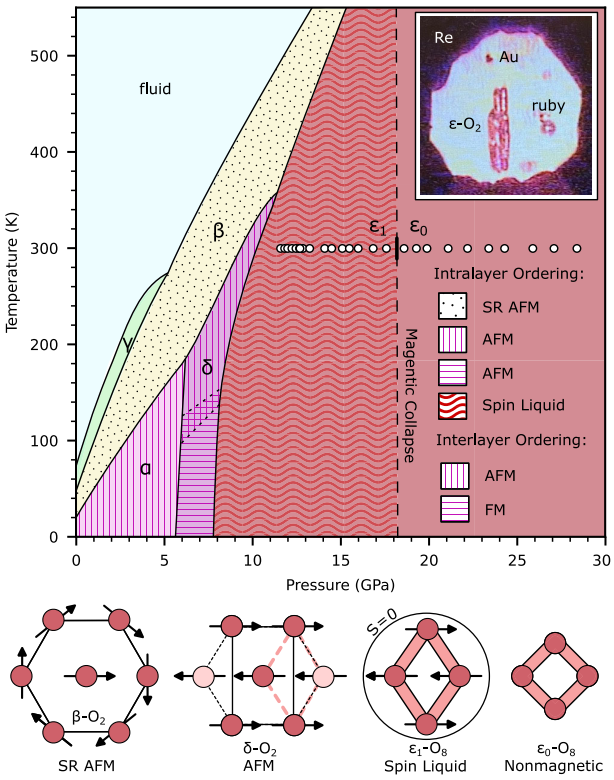

FIG. 1. High-pressure phase diagram of O_2 [1]. The type of order for the magnetically ordered phases are highlighted by the following: SR AFM, short-range antiferromagnetic; AFM, antiferromagnetic; and FM, ferromagnetic [4]. The single crystal refinements in this study are indicated by the empty circles. Solid and dashed black vertical lines represent the structurally evidenced transition between the spin liquid ($S = 1$), ϵ_1, and the spin zero ($S = 0$), ϵ_0, corresponding to the magnetic collapse. The ϵ_1-ϵ_0 phase boundary, although not explicitly calculated, was suggested to exhibit a positive slope [5]. Inset: photograph of the 10×2 μm ϵ-O_2 crystal in helium measured in this study.

of ϵ-O_2. Accompanying this transition, neutron diffraction confirms the collapse of antiferromagnetic order at the δ-ϵ boundary [4,19], consistent with spin pairing at the molecular level. Nevertheless, key spectroscopic anomalies persist, particularly the pronounced pressure-induced minimum in the IR O-O stretching frequency and its anomalous absorption enhancement [13], which remained unexplained by earlier simulation efforts [20].

A recent simulation study [5] proposed a model reconciling neutron diffraction and spectroscopic data through two isostructural ϵ-phase variants: ϵ_1 and ϵ_0. The ϵ_1 phase maintains O_2 molecular spin ($S = 1$) with short-range antiferromagnetic correlations in the $(O_2)_4$ tetramers, which have zero total spin, while the higher-pressure ϵ_0 phase (> 20 GPa) shows complete collapse of the O_2 molecular spin ($S = 0$) (see Fig. 1). The ϵ_1 phase represents a quantum solid with a spin-liquid-like singlet ground state arising from exchange coupling and fluctuations, consistent with the disappearance of long-range magnetic order at the δ-ϵ transition [4,19]. This model successfully reproduces spectroscopic anomalies via the ϵ_1-ϵ_0 magnetic collapse [5]. No ϵ_1-ϵ_0 structural transition has been observed in either powder [15] or single-crystal XRD studies [14]. This absence may reflect the transition's subtle magnetoelastic nature or experimental limitations—the single-crystal study (using He pressure medium) was restricted to 13–18 GPa with only three pressure points [14], while the powder XRD (conducted without pressure medium) might have masked minor structural changes.

To have a complete atomistic description of ϵ oxygen on compression so to be able to observe potential subtle structural changes correlated to the magnetic collapse proposed by simulations [5], we have performed structural refinements of a well-annealed ϵ-oxygen single crystals in He with an unprecedented accuracy, between 10 and 30 GPa at room temperature. We observe small concomitant discontinuities in two intra-O_8 distances, in the monoclinic angle, in the lattice parameter a, and a clear change in the volume equation of state at pressures of 17.6–18.6 GPa, whilst retaining the same $C2/m$ crystal structure. These small discontinuities, previously undetectable [14,15], can be manifestions of major changes in molecular spins that can be attributed to the ϵ_1-ϵ_0 transition at 18.1 ± 0.5 GPa proposed by calculations at comparable pressures [5].

A gas mixture containing 1% oxygen in helium was loaded at 1700 bar into diamond anvil cells equipped with Re gaskets. Oxygen single crystals were subsequently grown from the fluid mixture at 150 °C and 11–13 GPa by gradually cooling the system to room temperature (see Fig. S1 and the inset of Fig. 1). Pressures were measured by the ruby fluorescence method [21] or the gold equation of state [22]. We have repeatedly annealed the samples until an excellent crystal was obtained after several attempts, and all our single-crystal XRD patterns presented in this Letter were acquired on this crystal in the 10–30 GPa pressure range. Details on crystal annealing and characterization are provided in the End Matter and in Supplemental Material [23].

In Figs. 2 and S3, panels (a)–(c), we report the single-crystal refined structure ($C2/m$) of ϵ oxygen at a selected pressure of 12.24(4) GPa, shown along two different views, together with an enlargement of the $(O_2)_4$ unit. Key inter- and intracluster distances and angles labeled by D_x, d_x, and θ_x, respectively, are highlighted and their values vs pressure are reported in Fig. S3, panel (d), together with corresponding literature values [14]. Our refinement (12.24 GPa, Table I) was based on 215 measured reflections, of which 138 were unique reflections and 106 of these ones showed a signal-to-noise ratio larger than 2. The refinement resulted in an R factor of 2.7%. We confirm the structure proposed by Lundegaard *et al.* [14] based on O_8 units, but with one order of magnitude higher accuracy in determining atomic coordinates, which allows us to obtain an insight on the details of the structural changes with pressure. The O_8 unit is made by four collinear and coplanar O_2 molecules with

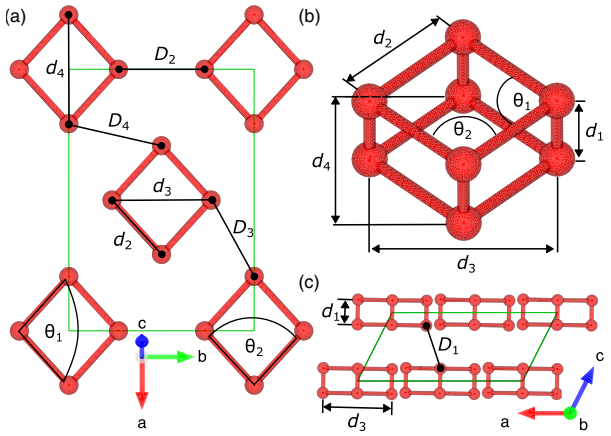

FIG. 2. Refined structure ($C2/m$) of ϵ oxygen at 12.24 GPa, with refinement details provided in Table I. Red balls: oxygen atoms. Red, thick lines connect groups of oxygen molecules forming the $(O_2)_4$ units. (a) Representation of a single plane of $(O_2)_4$ units that highlights key inter- and intracluster distances and angles labeled by D_x, d_x, and θ_x, respectively. (b) Enlargement of the $(O_2)_4$ unit with key intramolecular distances and angles labeled. (c) Representation of the ($C2/m$) unit cell orientated perpendicular to a-b plane making evident the monoclinic angle and shortest interlayer cluster distance, D_1 [25].

the centers of mass on the corners of an equilateral parallelogram, other than a square configuration. A similar refinement at a higher pressure, 19.92(2) GPa, is reported in Table I.

In Fig. 3, panel (a), we report the intracluster distances as a function of pressure, normalized to the values observed at 11.6 GPa, i.e., the interatomic O-O distance of the individual O_2 molecules (d_1), the O-O distance between two neighboring O_2 (d_2), which is the side of the rhombus, and the two diagonals of the rhombus (d_3 and d_4). We can readily observe a discontinuity at 18.1 ± 0.5 GPa of d_2 and d_4, also evidenced by a compression anisotropy consisting in a higher compression at low pressures followed by a lower compression terminating in the discontinuity. This is on the contrary not happening for d_3, which compresses almost linearly and without jumps in the same pressure range. The interatomic distance of the O_2 molecules is very little affected by the applied pressure as expected and compresses quite linearly. Yet, this compression is not entirely trivial. As a matter of fact, in principle, the pressure dependence of the O_2 bond length should be affected by two main contributions of opposite sign. One of these contributions should come from the strongly repulsive interactions between atoms belonging to different molecular layers, which in turn should reduce the bond length as the pressure increases. The other effect should result from the pressure enhanced charge transfer between the neighbor O_2 molecules. This effect reduces the intramolecular charge, thus weakening the corresponding bond and increasing its length. Clearly, the first effect prevails. In Fig. 3, panel (b), we report the pressure dependence of the ratio between the shorter (d_3) and the longer (d_4) diagonals of the O_8 rhombus. This ratio increases upon increasing pressure, reaching a maximum around 18 GPa. In other words, the rhombus becomes less and less elongated upon approaching this pressure. Similar changes in the shape of the O_8 cluster have been previously observed in structural data [26], albeit with a more scattered pressure dependence that likely obscured potential discontinuities in intracluster distances, which are clearly resolved in our study.

In Fig. 3, panels (c) and (d), we report the lattice parameters of ϵ oxygen as a function of pressure. We see that the a and b parameters are definitely more compressible than the c parameter. This is traced back to the fact that a and b are of pure intralayer nature, whereas c is partially related to the interlayer distance, which is stiffer due the repulsive interactions between atoms belonging to different layers. More importantly, each lattice parameter follows two different compression curves at pressures lower and higher than 18.1 ± 0.5 GPa, respectively. At pressures below this interval, while the fit of one-dimensional EOSs to the a, b, and c parameters was rather unsatisfactory (Fig. S4), second-order polynomials were instead found to fit all lattice parameters data very well (dashed curves). Clearly, the compression curves for the a lattice parameter and the β monoclinic angle show a saturation of the compression, i.e., an anomalous decrease in compressibility, the physical reason of which is not captured by one-dimensional EOS models and correlates with the saturation of the changes in the $(O_2)_4$ shape highlighted in panel (b) of Fig. 3. On the other hand, at pressures above 18.1 ± 0.5 GPa, 1D EOS models were found to fit very well the a, b, and c unit cell parameters, while a polynomial fit was still used for the β angle (continuous curves). Strikingly, the compression curves of the β and a lattice parameters exhibit discontinuities at 18.1 ± 0.5 GPa, similar to those observed for the intra-O_8 distances d_2 and d_4. These discontinuities measuring 0.09(1)° and 0.025(1) Å, respectively, are small yet clearly detectable, as they exceed their associated errors by at least one order of magnitude. These effects are indeed very subtle and can be detected thanks to the unprecedented accuracy of present measurements, whereas it was missed in previous XRD investigations [14,15]. In Fig. 3, panel (e), we also see that while our unit cell volume data vs pressure hardly fit to a single EOS (red line), these data instead fit well to a third-order Birch-Murnaghan (BM) EOS (3rd BM, dashed line) below 18.1 ± 0.5 GPa and to a distinct, stiffer, second-order Birch-Murnaghan EOS above this interval (2nd BM, continuous line). Parameters for these three EOS curves are reported in Table S1. A comparison between our volume data and literature data [14,15,24] is then presented in Fig. S5.

The reported discontinuities and changes in the compression curves at 18.1 ± 0.5 GPa clearly indicate the occurrence of a first-order isostructural phase transition that, at the present level of knowledge on the physics of solid oxygen, is more than natural to identify with the

TABLE I. Single-crystal refined structure ($C2/m$) of ϵ-oxygen [25].

Phase	ϵ_1-O_2	ϵ_0-O_2
Pressure (GPa)	12.24(4)	19.92(2)
Crystal size (μm)	2x2	2x2
Unit Cell:		
Space group:	$C2/m$	$C2/m$
a (Å)	8.0763(11)	7.6953(9)
b (Å)	5.7203(11)	5.4671(10)
c (Å)	3.7491(4)	3.6445(4)
β (°)	116.868(15)	116.104(14)
O_8-*cluster distances (Å):*		
O1-O1	1.2092(16)	1.205(3)
O1-O2	2.23835(17)	2.162(2)
O2-O3	1.2105(15)	1.204(2)
O1-O3	2.2851(17)	2.163(2)
Data collection:		
Number of measured reflections	215	182
Number of unique reflections	138	114
R_{int}	1.3%	3.2%
R_σ	2.7%	4.6%
Refinement details:		
$R(\text{I} > 2\sigma)$	2.7%	4.3%
$R(\text{all})$	3.4%	5.7%
Structure parameters:		
O1 (x,y,z)	0.036 79(12), 0.2667(2), 0.1808(2)	0.036 82(14), 0.2669(3), 0.1841(4)
O2 (x,y,z)	0.2487(2), 0.000 000, 0.1881(3)	0.2459(3), 0.000 000, 0.1925(5)
O3 (x,y,z)	0.1753(2), 0.000 000, -0.1738(3)	0.1724(3), 0.000 000, -0.1755(5)
O1 (U11, U22, U33, U23, U13, U12) (Å^2)	0.0257(7), 0.0239(10), 0.0149(6), −0.0021(2), 0.0076(4), −0.0019(3)	0.0191(9), 0.0171(13), 0.0097(10), −0.0013(3), 0.0057(5), −0.0014(3)
O2 (U11, U22, U33, U23, U13, U12) (Å^2)	0.0232(8), 0.0287(13), 0.0142(7), 0.000, 0.0051(6), 0.000	0.0176(10), 0.0173(16), 0.0098(11), 0.000, 0.0040(7), 0.000
O3 (U11, U22, U33, U23, U13, U12) (Å^2)	0.0255(8), 0.0252(13), 0.0142(7) 0.000, 0.0075(5), 0.000	0.0180(10), 0.0182(16), 0.0096(10), 0.000 0.0058(7), 0.000

predicted first-order isostructural ϵ_1-ϵ_0 phase transition [5]. Consistently, we suggest that the two structures observed below and above 18.1 ± 0.5 GPa belong to the ϵ_1 and ϵ_0 phases, respectively. As a consequence, we suggest that the observed transition corresponds to the long-sought magnetic collapse in ϵ oxygen, and the reason why it is of first order has been traced back to the mechanical coupling that the onset of molecular spin, which occurs upon entering ϵ_1 from ϵ_0, must exert on the overall crystal structure [5]. Following the same reasoning, the changes in the shape of the O_8 units described above, which we observed in the pressure domain of the ϵ_1 phase, are very likely of magnetoelastic origin. Related effects of similar origin were observed by looking at the b/a ratio, [Fig. 3, inset of panel (e)]. In fact, the increase of this ratio with increasing pressure was previously observed in the α and in the δ phases where it was interpreted as a magnetoelastic effect [29,30], which in turn is driven by the effective spin-spin Heisenberg exchange coupling that increases with pressure. Here, we found that the b/a ratio increases with pressure in the ϵ_1 phase as well, reaching a maximum at 15–18 GPa and then, upon entering the ϵ_0 phase, decreasing with further pressure increase. This nonmonotonic behavior clearly correlates with the magnetic collapse and we suggest it to be of magnetoelastic origin. In fact, the increase of the b/a ratio in the ϵ_1 phase is very likely due to the collective spin 1 singlet nature of this phase supporting magnetoelasticity, whereas the b/a ratio decreases upon entering the ϵ_0 just following the collapse of the spin and of the related magnetoelasticity. Incidentally, we note that the ϵ_1-ϵ_0 transition was predicted by DFT to occur at 20 GPa, at 0 K, with an unspecified error for the pressure [5]. This value is approximately 10% higher than our experimental result of 18.1 ± 0.5 GPa. Using thermodynamic arguments, these authors suggest that the ϵ_1-ϵ_0 phase boundary should have a positive slope, implying that the transition pressure at finite temperatures would likely exceed 20 GPa. However, no quantitative

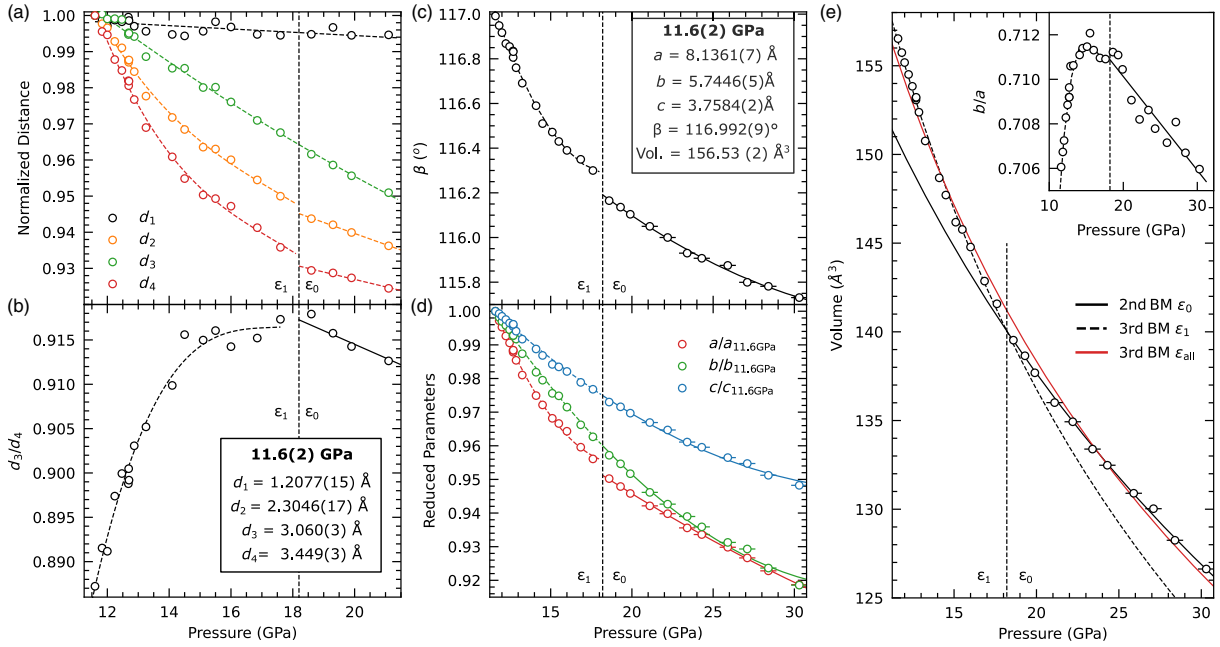

FIG. 3. Pressure dependence of structural parameters and equation of state of ϵ oxygen. (a) Intra-O_8 distances d_x, as defined in Fig. 2, reduced to the values observed at 11.6 GPa; (b) ratio between the shorter and the longer diagonal of the O_8 rhomboid; (c) β angle; (d) a, b, and c lattice parameters reduced to the values at 11.6 GPa; (e) unit cell volume; (e), inset, b/a ratio. Legends in panels (b) and (c) report values for d_x, lattice parameters, and unit cell volume measured at 11.6 GPa. Dashed vertical lines at 18.1 GPa in all panels correspond to simultaneous discontinuities in d_2, d_4, β, and a and to changes in the volume compression curve. These lines highlight the occurrence of the first order ϵ_1-ϵ_0 phase transition, which we interpret as the structural signature of the magnetic collapse. Curved dashed lines for d_x, d_3/d_4, a, b, c, and β and continuous line for β: guides for an eye, second-order polynomial fits through the experimental points. Continuous lines for a, b, and c: second-order Birch-Murnaghan fits to the data [27,28]. The dashed curve for the unit cell volume represents a third-order Birch-Murnaghan fit through the points of the ϵ_1 phase below 18.1 GPa, whereas the solid curve is a second-order Birch-Murnaghan [27,28] fit to the data above 18.1 GPa, corresponding to the ϵ_0 phase. The red curve represents a fit using a third-order Birch-Murnaghan equation of state (EOS) applied to all the data points. Parameters for the fits can be found in Table S1 in Supplemental Material [23]. For all panels, refinement-derived error bars are within the size of the symbols and the error on pressure is estimated to be at most ± 0.2 GPa and ± 0.5 GPa below and above 20 GPa, respectively.

estimates are provided for this scenario. Given the lack of detailed information and the uncertainty in the accuracy of DFT pressure predictions, it remains challenging to assess the extent to which the computed and experimentally observed transition pressures for the ϵ_1-ϵ_0 transition are quantitatively consistent. On the other hand, the quantitative results of the predictive study [5] align well to a large body of previous experimental spectroscopic data obtained at room temperature [13]. Notably, several anomalies observed experimentally between 18 and 20 GPa have been reinterpreted as evidence of magnetic collapse, which occurs in close proximity to the ϵ_1-ϵ_0 transition pressure observed in the present work.

We conducted synchrotron, single-crystal XRD investigations on the ϵ phase of solid oxygen at pressures of 11–30 GPa at room temperature. The unprecedented quality of our study, due to the careful sample preparation and to the high performances of the recently updated ID27-ESRF beam line, led us to reveal that the pressure domain of ϵ-O_2 actually parts in two isostructural subphases. The subphases are found to be connected through a first-order phase transition at 18.1 ± 0.5 GPa, while retaining the $(O_2)_4$ molecular units characteristic of ϵ oxygen. This transition is marked by small yet observable discontinuities in two intracluster distances and in the a and β lattice parameters, coinciding with abrupt changes in the unit cell volume EOS. The observation of two subphases in ϵ oxygen can be assigned to the recent model of oxygen's magnetic collapse, with the proposed ϵ_1 ($S = 1$) and ϵ_0 ($S = 0$) [5]. Importantly, the ϵ_1 phase was predicted to have a local spin-liquid-like singlet ground state rather than what would be a more energetic long-range, antiferromagnetic spin arrangement, which was also ruled out by recent neutron diffraction measurements searching for Bragg peaks of magnetic origin [4]. We remark that the subtle structural changes here found are driven by magneto-elasticity and, consequently, they are a valuable tool to observe the magnetic collapse in solid oxygen from the spin liquid ϵ_1 phase to the true diamagnetic ϵ_0 phase. This tool parallels and complements optical spectroscopy observations (see discussion in Ref. [5]), whereas direct observations of the magnetic state through magnetic susceptibility are nowadays a technological unattainable challenge. Finally, the entire P-T ϵ_1-ϵ_0 phase boundary and whether this line ends at a critical point, as was predicted [5], remain to be experimentally investigated.

Acknowledgments—We acknowledge the European Synchrotron Radiation Facility for provision of beam time at ID27 (proposal CH-5607 and CH-6300). M. S. acknowledges HPSTAR for having allowed him as a Visiting Scientist during part of his research on solid oxygen.

Data availability—The data that support the findings of this article are openly available [25].

[1] Yu A. Freiman, H. J. Jodl, and Yanier Crespo, Solid oxygen revisited, Phys. Rep. **743**, 1 (2018).
[2] Yu A. Freiman and H. J. Jodl, Solid oxygen, Phys. Rep. **401**, 1 (2004).
[3] R. LeSar and R. D. Etters, Character of the α-β phase transition in solid oxygen, Phys. Rev. B **37**, 5364 (1988).
[4] Stefan Klotz, Magnetism in solid oxygen studied by high-pressure neutron diffraction, J. Low Temp. Phys. **192**, 1 (2018).
[5] Yanier Crespo, Michele Fabrizio, Sandro Scandolo, and Erio Tosatti, Collective spin 1 singlet phase in high-pressure oxygen, Proc. Natl. Acad. Sci. U.S.A. **111**, 10427 (2014).
[6] C. A. English and J. A. Venables, The structure of diatomic molecular solids, Proc. R. Soc. A **340**, 57 (1974).
[7] S. Serra, G. Chiarotti, S. Scandolo, and E. Tosatti, Pressure-induced magnetic collapse and metallization of molecular oxygen: The ζ-O_2 phase, Phys. Rev. Lett. **80**, 5160 (1998).
[8] G. Weck, P. Loubeyre, R. LeToullec, and R. LeToullec, Observation of structural transformations in metal oxygen, Phys. Rev. Lett. **88**, 035504 (2002).
[9] Philip Dalladay-Simpson, Bartomeu Monserrat, Li Zhang, and Federico Gorelli, Distinct vibrational signatures and complex phase behavior in metallic oxygen, Matter Radiat. Extremes **9**, 028401 (2024).
[10] Yuichi Akahama, Haruki Kawamura, Daniel Häusermann, Michael Hanfland, and Osamu Shimomura, New high-pressure structural transition of oxygen at 96 GPa associated with metallization in a molecular solid, Phys. Rev. Lett. **74**, 4690 (1995).
[11] Yuichi Akahama, Haruki Kawamura, and Osamu Shimomura, Structural phase transitions of solid oxygen at low temperature and high pressure, Phys. Rev. B **64**, 054105 (2001).
[12] Alexander F. Goncharov, N. Subramanian, T. R. Ravindran, Maddury Somayazulu, Vitali B. Prakapenka, and Russell J. Hemley, Polymorphism of dense, hot oxygen, J. Chem. Phys. **135**, 084512 (aug 2011).
[13] Federico A. Gorelli, Lorenzo Ulivi, Mario Santoro, and Roberto Bini, The ϵ phase of solid oxygen: Evidence of an O_4 molecule lattice, Phys. Rev. Lett. **83**, 4093 (nov 1999).
[14] Lars F. Lundegaard, Gunnar Weck, Malcolm I. McMahon, Serge Desgreniers, and Paul Loubeyre, Observation of an O_8 molecular lattice in the ϵ phase of solid oxygen, Nature (London) **443**, 201 (2006).
[15] Hiroshi Fujihisa, Yuichi Akahama, Haruki Kawamura, Yasuo Ohishi, Osamu Shimomura, Hiroshi Yamawaki, Mami Sakashita, Yoshito Gotoh, Satoshi Takeya, and Kazumasa Honda, O_8 cluster structure of the Epsilon phase of solid oxygen, Phys. Rev. Lett. **97**, 085503 (2006).
[16] Yue Meng, Peter J. Eng, John S. Tse, Dawn M. Shaw, Michael Y. Hu, Jinfu Shu, Stephen A. Gramsch, Chichang Kao, Russell J. Hemley, and Ho-Kwang Mao, Inelastic x-ray scattering of dense solid oxygen: Evidence for intermolecular bonding, Proc. Natl. Acad. Sci. U.S.A. **105**, 11640 (2008).
[17] Jeremy K. Burdett and Stephen Lee, Peierls distortions in two and three dimensions and the structures of AB solids, J. Am. Chem. Soc. **105**, 1079 (1983).
[18] Malcolm Nicol, K. R. Hirsch, and Wilfried B. Holzapfel, Oxygen phase equilibria near 298 K, Chem. Phys. Lett. **68**, 49 (1979).
[19] I. N. Goncharenko, Evidence for a magnetic collapse in the epsilon phase of solid oxygen, Phys. Rev. Lett. **94**, 205701 (2005).
[20] J. B. Neaton and N. W. Ashcroft, Low-energy linear structures in dense oxygen: Implications for the epsilon phase, Phys. Rev. Lett. **88**, 205503 (2002).
[21] Guoyin Shen, Yanbin Wang, Agnes Dewaele, Christine Wu, Dayne E. Fratanduono, Jon Eggert, Stefan Klotz, Kamil F. Dziubek, Paul Loubeyre, Oleg V. Fat'yanov, Paul D. Asimow, Tsutomu Mashimo, and Renata M. M. Wentzcovitch, Toward an international practical pressure scale: A proposal for an ipps ruby gauge (ipps-ruby2020), High Press. Res. **40**, 299 (2020).
[22] Yingwei Fei, Angele Ricolleau, Mark Frank, Kenji Mibe, Guoyin Shen, and Vitali Prakapenka, Toward an internally consistent pressure scale, Proc. Natl. Acad. Sci. U.S.A. **104**, 9182 (2007).
[23] See Supplemental Material at http://link.aps.org/supplemental/10.1103/jvd7-v9h9 for additional information about details on crystal annealing and characterization, which includes Refs. [14,15,21,24].
[24] G. Weck, S. Desgreniers, P. Loubeyre, and M. Mezouar, Single-crystal structural characterization of the metallic phase of oxygen, Phys. Rev. Lett. **102**, 255503 (2009).
[25] CSD 2388426-2388446 contains the supplementary crystallographic data for this Letter. These data are provided free of charge by the joint Cambridge Crystallographic Data Centre and Fachinformationszentrum Karlsruhe Access Structures service; F. A. Gorelli, M. Santoro, P. Dalladay-Simpson, and J. Haines, "Single crystal XRD investigation of a critical point terminated phase boundary in solid oxygen (2022)" [Dataset], European Synchrotron Radiation Facility, 10.15151/ESRF-ES-817610854 and 10.15151/ESRF-ES-988988001.
[26] Yuichi Akahama, Hiroshi Fujihisa, Naohisa Hirao, and Yasuo Ohishi, Relation between O_8 cluster shape and vibrational spectra in the epsilon-phase of solid oxygen, Jpn. J. Appl. Phys. **58**, 095502 (2019).

[27] Francis Birch, Finite elastic strain of cubic crystals, Phys. Rev. **71**, 809 (1947).
[28] Javier Gonzalez-Platas, Matteo Alvaro, Fabrizio Nestola, and Ross Angel, EosFit7-GUI: A new graphical user interface for equation of state calculations, analyses and teaching, J. Appl. Crystallogr. **49**, 1377 (2016).
[29] Federico A. Gorelli, Mario Santoro, Lorenzo Ulivi, and Michael Hanfland, Crystal structure of solid oxygen at high pressure and low temperature, Phys. Rev. B **65**, 1721061 (2002).
[30] R. D. Etters, K. Kobashi, and J. Belak, Calculated properties of solid O_2 under pressure at low temperature, Phys. Rev. B **32**, 4097 (1985).
[31] S. Klotz, J.-C. Chervin, P. Munsch, and G. Le Marchand, Hydrostatic limits of 11 pressure transmitting media, J. Phys. D **42**, 075413 (2009).
[32] Clemens Prescher and Vitali B. Prakapenka, Dioptas: A program for reduction of two-dimensional x-ray diffraction data and data exploration, High Press. Res. **35**, 223 (2015).
[33] Oxford (UK) Rigaku Oxford Diffraction, Crysalispro software system (2021).
[34] George M. Sheldrick, Crystal structure refinement with SHELXL, Acta Crystallogr. Sect. C **71**, 3 (2015).

End Matter

Appendix—Oxygen single crystals were grown from the He/O_2 fluid mixture at 150 °C and 11–13 GPa by gradually cooling the system to room temperature (see Fig. S1 and the inset of Fig. 1). We have repeatedly annealed the sample until an excellent crystal was obtained after several attempts. After each annealing cycle, the quality of the newly grown crystal was assessed based on the single-crystal XRD data structure refinements, as visual inspection alone was insufficient to evaluate the crystal quality. XRD data were collected using spatial steps of 2 μm to identify a region corresponding to a unique single-crystal domain with a consistent orientation matrix and no unindexed reflections from potential secondary domains. Our final, best crystal exhibited a needlelike morphology with dimensions of approximately 10 μm in length and 2 μm in width (Fig. 1, inset) and contained two single-crystal domains. We then acquired single-crystal XRD patterns at numerous pressure points between 10 and 30 GPa (Fig. 1), always probing the same domain of the crystal at each pressure, with fine pressure increments that were allowed to stabilize. The sample was not annealed again along the pressure scan, and the quality of the investigated single-crystal domain remained consistent up to approximately 21 GPa, which allowed us to extract all the structural parameters up to this pressure. Above this point, it was still possible to extract lattice parameters with a high accuracy, although a slight degradation of the single-crystal domain prevented us from obtaining reliable values for the atomic positions as the number of observed reflections was already reduced by 2 and the R_{int} factor was already greater than 25% by 23 GPa. This degradation also prevented us from performing accurate structural measurements upon reducing pressure. Interestingly, the FWHM of the $R1$ ruby line used for pressure measurements increased by at most 3% from 11.6 to 22–23 GPa, while it increased by 13% further increasing the pressure to 30 GPa (Fig. S2). This parallels previous studies where standard deviation of the pressures measured by several ruby spheres in helium is stable up to about 23 GPa [31], which in turn is consistent with conservation of high quality oxygen single crystal in He up to similar pressures in the present work. Further details on crystal annealing and characterization are provided in Supplemental Material [23]. XRD patterns were measured at the ID27 beam line of the ESRF, using the EIGER2 X CdTe 9M area detector and monochromatic radiation ($\lambda = 0.3738$ Å) focused to 0.5 μm size beam spot diameter, to select and probe points of the sample smaller than the individual single-crystal domains studied. The diffractoxmeter was calibrated using vanadinite and CeO_2 for single-crystal and powder XRD measurements, respectively. Dioptas software was used to integrate 2D diffraction images to 1D patterns [32]. Single-crystal datasets were collected by acquiring diffraction intensities in the ω-oscillation scan mode with $\pm 32°$ range, 0.5° frame width and 1 s exposure per frame and the diffraction data were processed using CrysAlisPro [33], including corrections for Lorentz and polarization effects, as well as multiscan absorption correction. No evidence for twinning, satellite reflections, or diffuse scattering in the domain investigated was found by visual inspection of the area detector images. The structure was refined using SHELXL-2017/1 [34].